CFD Modeling of Flow Patterns and Hydraulics of Commercial-Scale Sieve Trays

Getye Gesit, K. Nandakumar, and K. T. Chuang
Dept. of Chemical and Materials Engineering, University of Alberta, Edmonton, AB, T6G 2G6, Canada

A computational fluid dynamics (CFD) model was used to predict the flow patterns and hydraulics of a commercial-scale sieve tray. The model considers the 3-D two-phase flow of gas and liquid in which each phase is treated as an interpenetrating continuum having separate transport equations. Interaction between the two phases occurs via an interphase momentum transfer. For the CFD analysis, the commercial packages CFX5.4 and CFX4.4 of AEA Technology were employed. Velocity distributions, clear liquid height, froth height, and liquid holdup fraction in froth were predicted for various combinations of gas and liquid flow rates. Tray geometry and operating conditions were based on the experimental work that Solari and Bell carried out in a 1.22-m diameter air–water simulator in 1986 at Fractionation Research Inc. Predicted results were found to be in good agreement with the experimental data of these authors. The objective of the work was studying the extent to which CFD can be used as a prediction and design tool for industrial trays. The simulation results are such that CFD can be used as an invaluable tool in tray design and analysis.

Introduction

Sieve trays are widely used as phase-contacting devices in distillation, absorption, and liquid–liquid extraction columns. An impasse that has hindered the further improvement of these devices is the fact that little is known about the flow phenomena prevailing inside a tray for given geometry and operating conditions. The main reason for this is the poor understanding of the complex behaviors of the multiphase flow inside the tray. As a result, current design and analysis of trays are based on experience and empirical correlations. These practices do not often take into account the actual fluid flow patterns. For example, the well-known AIChE tray design procedure assumes a uniform rectilinear velocity field with transverse mixing. However, experimental studies (Bell, 1972; Weiler et al., 1973; Sohlo and Kinnunen, 1977; Solari et al., 1982; Solari and Bell, 1986) have shown that actual flow patterns found on industrial trays include flow maldistributions such as channeling, recirculation, stagnant zones, and nonuniform velocity distributions. Except for the few case reports, little is known about what flow configuration to expect for given tray geometry and operating conditions. Mathematical models such as those of Porter et al. (1972), Bell and Solari (1974), Solari and Bell (1978) show that flow maldistributions can reduce tray efficiency. Only two attempts (Solari et al., 1982; Solari and Bell, 1986) have been made to relate model parameters to tray geometry and fluid rates, and it is not known if these model parameters could be extended to other tray geometries and fluid systems. Very little experimental work has been done to assess the effect of flow maldistributions on tray efficiency.

Therefore, there are two major unresolved problems facing the current practice of tray design and analysis. The first one is what flow patterns to expect for given geometry and operating conditions. The second problem is how to relate these flow patterns to tray performance parameters such as tray efficiency and pressure drop. Once a method or methods are devised to accomplish the two tasks, it will be possible to design trays that have the desired flow patterns that give rise to the best performance. Over the past years, only experimental methods could be thought of to solve the problems mentioned. Although experimental predictions are generally expected to give reliable data, the chaotic, three-dimensional and multiphase behaviors of the flow inside a tray severely limit the use of these methods and the amount of data they can give.

Correspondence concerning this article should be addressed to K. T. Chuang.

Recently, the development of powerful computers, advances in numerical methods, and improvements in multiphase flow models permit investigation of complex flow problems (Mehta et al., 1998). The technique that combines these is computational fluid dynamics (CFD), a technique that is emerging as an important predictive and design tool for flows in process equipment. Compared to experimental methods, it gives complete information, and has a relatively low cost and a fast speed. A further major advantage of CFD over experimental methods is its flexibility, as it typically enables changing flow geometry and system conditions without incurring appreciable cost. An important step should, however, accompany the first time use of CFD; its extent of applicability has to be validated using experimental data mainly to cater for uncertainties involved in mathematically and numerically modeling complex flow phenomena such as turbulence and multiphase interactions.

About four attempts have been made so far to simulate tray hydrodynamics using CFD. In a previous work (Mehta et al., 1998), liquid-velocity distributions were predicted by considering the steady-state, three-dimensional flow of the liquid phase. The effects of the vapor flow were taken into account by incorporating additional terms calculated using empirical correlations for sieve tray hydraulics. Fischer and Quarini (1998) modeled the three-dimensional transient gas–liquid tray hydrodynamics by using a drag coefficient with a constant value of 0.44, a value that corresponds to the inertial turbulent regime. Liu et al. (1999) developed a two-dimensional model that simulates the flow of the liquid phase. They have attempted to include the effect of the vapor flow by incorporating additional terms into the liquid-phase model equations. Krishna et al. (1999b) for a rectangular geometry and van Baten and Krishna (2000) for a circular geometry developed CFD models to simulate the transient, three-dimensional two-phase flow behavior of a 0.3-m-dia. sieve tray. The two-phase equations were coupled through an interphase drag term that was estimated using the drag coefficient correlation of Krishna et al. (1999a) and the Bennett et al. (1983) correlation for liquid holdup fraction in froth. The authors reported clear-liquid height and dispersion profile predictions, and remarked that the flow inside the tray exhibited a chaotic and three-dimensional behavior.

Van Baten and Krishna (2000) have done excellent work in using a CFD model to simulate sieve tray hydrodynamics. The authors focused primarily on the prediction of tray hydraulics; namely, on predicting clear-liquid height and dispersion density. They made no attempt to predict and validate fluid flow patterns, the prediction of which remains the main problem in tray analysis and design. Their tray geometry is small scale. In this work, a CFD model has been developed to predict the flow patterns and hydraulics of a commercial-scale sieve tray. This extends the previous single-phase simulation to a two-phase one. We give the predictions of both the fluid flow patterns and hydraulics of the complete sieve tray including the downcomer region. The interphase momentum drag term that couples the gas- and liquid-phase transport equations was calculated by using the drag coefficient estimate of Krishna et al. (1999a) and an average gas holdup fraction correlation. The correlations of Bennett et al. (1983) and Colwell (1979) were considered for the average gas holdup fraction. Tray geometry and fluids were based on the experimental work of Solari and Bell (1986) carried out at the Fractionation Research Inc. in a 1.22-m air–water simulator. We made predictions of velocity distributions, clear-liquid height, froth height, and liquid holdup fraction in froth. The CFD simulation results are in good agreement with the experimental results of Solari and Bell (1986). Our objective has been to find the extent to which CFD can be used as a design and prediction tool for industrial trays. From the results of this work, we conclude that CFD can be used as an invaluable tool in tray design and analysis.

Model Equations

The model considers the flow of gas and liquid in the Eulerian–Eulerian framework in which each phase is treated as interpenetrating continuum having separate transport equations. With the model focusing on the froth region of the sieve tray, the gas phase has been taken as the disperse phase, while the liquid phase has formed the continuous phase. Since the focus is on the hydrodynamic behavior of sieve trays, energy and mass transfers have not been considered in this work. The system being modeled is that used by Solari and Bell (1986)—viz., the air–water system. Thus, for each phase the time and volume averaged continuity and momentum equations are numerically solved. Jacobson et al. (1997) have considered the derivation of the multiphase flow transport equations. The monographs by Gidaspow (1994) and Crowe et al. (1998) present a critical view of the multiphase flow models.

Continuity equations

Gas phase

$$\frac{\partial(r_G \rho_G)}{\partial t} + \nabla\cdot(r_G \rho_G V_G) = 0 \tag{1}$$

Liquid phase

$$\frac{\partial(r_L \rho_L)}{\partial t} + \nabla\cdot(r_L \rho_L V_L) = 0 \tag{2}$$

Momentum equations

Gas phase

$$\frac{\partial}{\partial t}(r_G \rho_G V_G) + \nabla\cdot(r_G(\rho_G V_G V_G)) = -r_G \nabla p_G + \nabla\cdot\left(r_G \mu_{\text{eff},G}\left(\nabla V_G + (\nabla V_G)^T\right)\right) - \boldsymbol{M}_{GL} \tag{3}$$

Liquid phase

$$\frac{\partial}{\partial t}(r_L \rho_L V_L) + \nabla\cdot(r_L(\rho_L V_L V_L)) = -r_L \nabla p_L + \nabla\cdot\left(r_L \mu_{\text{eff},L}\left(\nabla V_L + (\nabla V_L)^T\right)\right) + \boldsymbol{M}_{GL} \tag{4}$$

The gas and liquid volume fractions, r_G and r_L, are related by the summation constraint

$$r_G + r_L = 1. \tag{5}$$

The same pressure field has been assumed for both phases, that is, $p_G = p_L$.

The effective viscosities of the gas and liquid phases are $\mu_{\text{eff},G}$ and $\mu_{\text{eff},L}$, respectively

$$\mu_{\text{eff},G} = \mu_{laminar,G} + \mu_{\text{turbulent},G} \tag{6}$$

$$\mu_{\text{eff},L} = \mu_{laminar,L} + \mu_{\text{turbulent},L} \tag{7}$$

The term $\boldsymbol{M}_{GL}$ in the momentum equations represents interphase momentum transfer between the two phases.

Closure relationships

In order to solve Eqs. 1 to 4 uniquely for velocities, pressure, and volume fractions, we need additional equations that relate the interphase momentum transfer term $\boldsymbol{M}_{GL}$ and the turbulent viscosities to the mean flow variables. The interphase momentum transfer term $\boldsymbol{M}_{GL}$ is basically interphase drag force per unit volume. With the gas as the disperse phase, the equation for $\boldsymbol{M}_{GL}$ is

$$\boldsymbol{M}_{GL} = \frac{3}{4}\frac{C_D}{d_G} r_G \rho_L |\boldsymbol{V}_G - \boldsymbol{V}_L|(\boldsymbol{V}_G - \boldsymbol{V}_L) \tag{8}$$

The drag coefficient, C_D, has been estimated using the drag correlation of Krishna et al. (1999a), a relation proposed for the rise of a swarm of large bubbles in the churn turbulent regime

$$C_D = \frac{4}{3}\frac{\rho_L - \rho_G}{\rho_L} g d_G \frac{1}{V_{\text{slip}}^2} \tag{9}$$

where the slip velocity, $V_{\text{slip}} = |\boldsymbol{V}_G - \boldsymbol{V}_L|$, is estimated from the gas superficial velocity, V_S, and the average gas holdup fraction in the froth region is estimated as

$$V_{\text{slip}} = \frac{V_S}{r_G^{\text{average}}} \tag{10}$$

For the average gas holdup fraction, two correlations were considered. One was the correlation of Bennett et al. (1983)

$$r_G^{\text{average}} = 1 - \exp\left[-12.55\left(V_S\sqrt{\frac{\rho_G}{\rho_L - \rho_G}}\right)^{0.91}\right] \tag{11}$$

The second one was Colwell's (1979)

$$r_G^{\text{average}} = 1 - \frac{1}{1 + 12.6\left[\left(\frac{\rho_G}{\rho_L - \rho_G}\right)\frac{V_S^2}{g h_L}\right]^{0.4}\left(\frac{A_H}{A_B}\right)^{-0.25}} \tag{12}$$

Substituting and simplifying, the interphase momentum transfer term as a function of local variables and constant coefficients put in a form suitable for CFD use becomes (van Baten and Krishna, 2000)

$$\boldsymbol{M}_{GL} = \frac{\left(r_G^{\text{average}}\right)^2}{\left(1.0 - r_G^{\text{average}}\right)V_S^2} g(\rho_L - \rho_G) r_G r_L |\boldsymbol{V}_G - \boldsymbol{V}_L|(\boldsymbol{V}_G - \boldsymbol{V}_L) \tag{13}$$

Interestingly this relation is independent of bubble diameter. This obviates the need for its input that could have been difficult.

The turbulence viscosities were related to the mean flow variables by using the standard k-ϵ turbulence model with default model coefficients. No turbulence models were used for the gas phase. The k-ϵ model is well treated in the literature (Wilcox, 1993; Libby, 1998; Salas et al., 1999; and Pope, 2000). Banerjee (1990) analyzes the modeling considerations for turbulent multiphase flows. Borchers et al. (1999) have assessed the applicability of the k-ϵ model for gas–liquid flows in bubble columns.

Flow Geometry

The model geometry and boundaries are shown in Figure 1. The tray has a diameter of 1.22 m, a 13% downcomer area, a weir height of 0.05 m, a downcomer clearance of 0.038 m, and a 5% hole area with 0.0127-m-diam holes arranged in a 0.05-m triangular pitch. Solari et al. (1982) and Solari and Bell (1986) found symmetric flow fields about the tray center. Making use of their observations, only half of the tray was modeled so as to save computational time and machine memory. The model includes the downcomer region. Liquid enters the tray through the downcomer clearance area, labeled Liquid Inlet, and leaves the flow geometry through the downcomer clearance area that leads to the tray below, labeled

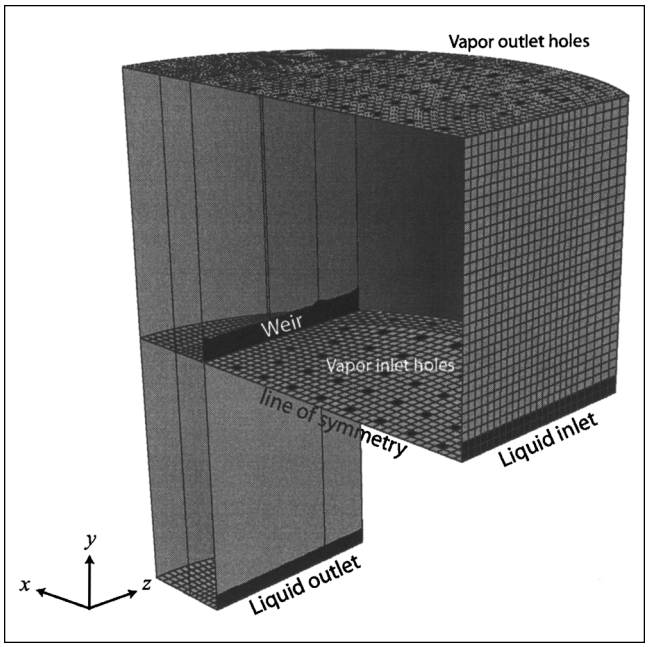

Figure 1. Flow geometry and boundary conditions.

Plane $z = 0$ is a plane of symmetry.

Liquid Outlet. Gas enters through holes at the bottom of the tray, labeled Vapor Outlet, and leaves through holes at the top, labeled Vapor Outlet.

One of the geometry modeling problems we faced was specifying the gas inlet and outlet holes. Because of the relatively large tray diameter we had, working with the actual number of holes proved to be computationally demanding. Hence, in several simulations we use a smaller number of holes, the total area of which equals that of the total area of the actual number of holes. However, in a few simulations (using CFX 5.4, which uses an unstructured grid and a coupled solver) we did use the actual number of holes, and we compare the flow predictions on both the macro (like froth height) and micro (velocity distributions) scales. In some simulations, we also tried to do away with the holes entirely and specify a uniform vapor velocity at the bottom vapor inlet, but it proved to be unsatisfactory.

The whole tray spacing (0.61 m) was considered in the simulation, even though the primary focus is in the froth region (about 0.20 m above the tray floor). This resulted in a better numerical convergence, as well as providing us with the ability to assess the froth height from the simulations.

Boundary and Initial Conditions

Boundary conditions

To solve the continuity and momentum equations, appropriate boundary conditions must be specified at all external boundaries plus at any specific internal boundaries of the flow geometry. Unfortunately, there is a lack of information about the inlet flow conditions in the sieve tray literature; only average quantities like the flow rate are measured, while the simulation requires a detailed velocity profile as the input. We were guided by intuition and experience in specifying the boundary conditions. In some cases, an iterative procedure was followed where the results of a specified boundary profile were compared against the experimental data for the interior points of the tray.

Liquid inlet

The velocity profile at the liquid inlet was found to have a significant effect on the liquid velocity distribution inside the tray. In the single-phase modeling work (Mehta et al., 1998), a uniform liquid inlet velocity profile was recommended for low values of the flow parameter, F_{LV} ($F_{LV} < 0.25$). That was found to be an important recommendation. Equations 14 and 15 give the two liquid inlet velocity profiles tested and used in this work.

Uniform Liquid Inlet Velocity Profile.

$$U_{L,\text{in}} = \frac{Q_L}{A_{CL}} \tag{14}$$

Parabolic Liquid Inlet Velocity Profile.

$$U_{L,\text{in}} = \frac{1.5Q_L}{A_{CL}}\left[1 - \left(\frac{2z}{L_W}\right)^2\right] \tag{15}$$

with $A_{CL} = h_{\text{ap}} L_W$, where h_{ap} is the downcomer clearance or apron and L_W is the weir length. The liquid-volume fraction at the liquid inlet was taken to be unity, assuming that only liquid enters through the downcomer clearance. This is not a bad approximation, since the amount of vapor entrainment is small.

Vapor inlet

The gas inlet and outlet holes of the model are individual cell faces at the bottom and top of the tray. Because of the cylindrical geometry of the tray and the tapering at the weir location, the structured grid gives cell faces that differ in areas. The gas velocity at an inlet hole was calculated such that the same mass flow rate enters through each hole

$$V_{\text{hole},i} = \left(\frac{V_S A_B}{2N_H}\right)\frac{1}{A_{\text{hole},i}} \tag{16}$$

where N_H is the number of holes in the model geometry (half of the full tray). The gas-hole velocity, thus, depends on the size and number of holes, although their products make the changes in the hole-velocity values less sensitive. Another way of specifying the gas-hole velocities is to specify the same gas-hole velocity for the inlet holes

$$V_{\text{hole}} = \frac{V_S A_B}{2\sum_{i=1}^{N_H} A_{\text{hole},i}} \tag{17}$$

For a given inlet hole, the ratio of the gas momentum calculated using Eq. 16 to that calculated using Eq. 17 will be

$$\left(\frac{V_{\text{hole},i}}{V_{\text{hole}}}\right)^2 = \left(\frac{\sum_{i=1}^{N_H} A_{\text{hole},i}}{N_H A_{\text{hole},i}}\right)^2 \tag{18}$$

The closer the hole-area values are, the more uniform the gas bubbling becomes. Neither of the equations for the gas-hole velocity assures uniform gas bubbling. The gas volume fraction at the inlet holes was specified to be unity.

Liquid and vapor outlets

The liquid- and vapor-outlet boundaries were specified as mass flow boundaries with fractional mass flux specifications. At the liquid outlet, only liquid was assumed to leave the flow geometry and only gas was assumed to exit through the vapor outlet. These specifications are in agreement with the specifications at the gas inlet and liquid inlet, where only one fluid was assumed to enter.

Wall and symmetry boundary conditions

A no-slip wall boundary condition was specified for the liquid phase and a free slip wall boundary condition was used for the gas phase. At the plane of symmetry, the normal velocity is zero and the gradients of the other variables in the transverse coordinate direction are taken to be zero.

Flow-field initialization

Good initial guesses of the flow variables are important not only to avoid a significantly longer computational time but also in some cases to avoid divergence. Water and air at room temperature and atmospheric pressure were the fluids used in the simulation. Initially, we filled the tray with water and air having volume fractions that varied in the vertical direction. In order to shorten the time needed to reach convergence, volume fractions were estimated using functions whose parameters were determined using sieve tray hydraulics correlations. For both of the regions above the bubbling area of the tray and the downcomer, functions of the following form were employed

$$r_{L1} = r_0 \quad \text{if} \quad y \le h_L \tag{19}$$

$$r_{L2} = a + by^c \quad \text{if} \quad y \ge h_L \tag{20}$$

where r_0 is a constant value set slightly greater than the average liquid holdup fraction in the froth region calculated using the Bennett et al. correlation. Typically values ranging from 0.8 to 0.9 were used, depending on the liquid and gas rates. The constants a, b, and c were determined by requiring the equation to satisfy three conditions. One was that the equation should return $r_L = r_0$ at $y = h_L$. This was done to avoid sudden localized jumps in the volume-fraction values. The second one was that the equation should return $r_L = 0.1$ at $y = h_F$. The last requirement was that the following integral sum should hold

$$T_S\left[\frac{1}{h_L}\int_0^{h_L} r_{L1}(y)\,dy + \frac{1}{(T_S - h_L)}\int_{h_L}^{T_S} r_{L2}(y)\,dy\right] = h_L \tag{21}$$

For the downcomer region, the clear-liquid height is equal to the downcomer backup, and a value of 0.99 was used for r_0.

The superficial gas velocity based on the bubbling area was used as an initial guess for the vertical component of the gas velocity throughout the flow region. The other components of the gas velocity were set to zero. For the liquid phase, a uniform horizontal velocity distribution that is equal to the flat liquid inlet velocity value was specified for all the cells in the froth region. A small negative value was set for the vertical component of the liquid velocity in the froth region. In the downcomer region, the downcomer velocity of the liquid was specified for the vertical component of the liquid velocity.

Simulation Results

Solution algorithms

The CFD analysis was carried out using the commercial packages CFX5.4 and CFX4.4 of AEA Technology. Transient simulations were conducted in CFX4.4, while those of the CFX5.4 were steady-state ones. In CFX4.4, hybrid differencing was used for all the equations except for the volume-fraction equations where the Min-Mod scheme (van Leer, 1974) was used. For the time term, implicit first-order backward time differencing was used with fixed time steps that varied from 5.0×10^{-4} s to 5.0×10^{-3} s. We found it necessary to run simulations with small underrelaxation factors generally less than 0.5. Most of the transient simulations were conducted using eight SGI R10000 195-MHz processors run in parallel. Better transient simulation convergence was observed when starting with lower gas rates. Tray hydraulics parameters such as clear-liquid height and froth height were calculated at each time step. A transient simulation was deemed to have converged whenever the clear-liquid height value showed no appreciable change with time. Although many of the simulations were inherently transient, an averaged quantity like the clear-liquid height appears to have reached a steady value, as seen in Figure 2. Such indicators were used to terminate a simulation, even if local values were changing with time in a bounded, chaotic manner. Several simulations were conducted with CPU time per CFD simulation for convergence varying from as low as half a day to about a week.

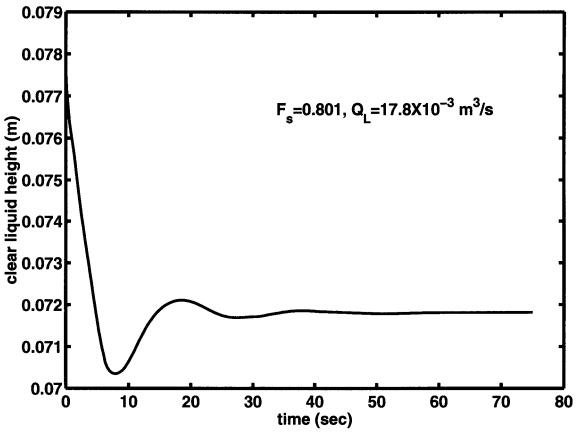

Figure 2. Transient simulation convergence as indicated by a plot of clear liquid height vs. time.

A transient simulation is assumed to have converged whenever the clear-liquid height does not appreciably change with time.

Grid-size sensitivities

Grid convergence requires that after a certain grid size the numerical results should not change significantly as the grid size is further decreased. Because of the relatively large tray diameter used, it was necessary to work with relatively coarse meshes that had a small number of vapor inlet holes. The sensitivities of the simulation results to grid size, the number of holes and their size, have been checked for both the structured (CFX4.4) and the unstructured (CFX5.4) meshes. For the CFX4.4 simulations, an eight-block grid structure was constructed to get finite volume cells with higher orthogonalities. Test simulations were run with a coarse grid of 10,692 cells having 18 holes. We checked the sensitivity of the simulation results by comparing the results for 10,692, 32,784, and 42,716 cells (Figures 3 and 4). Figure 3 shows a macroscopic quantity, viz., clear liquid height for three different grid sizes, while Figure 4 shows detailed velocity variation along two locations in the tray. This figure also includes the experimental data points as measured by Solari and Bell (1986). The authors made linear liquid-velocity measurements along two

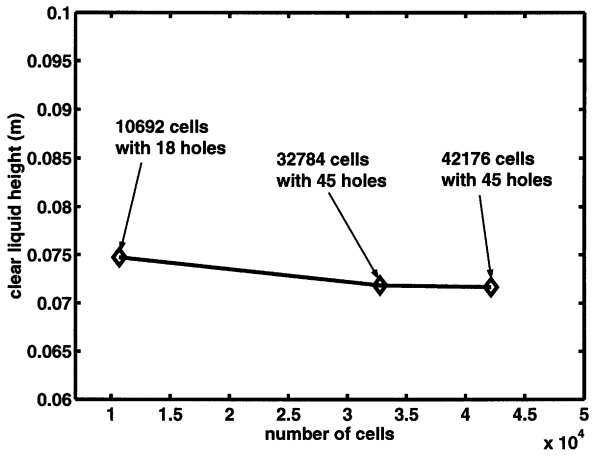

Figure 3. Sensitivity of the clear liquid height prediction to grid spacing, and hole number and size, $Q_L = 6.94 \times 10^{-3}$ m^3/s, $F_S = 0.462$ (CFX4.4).

lines perpendicular to the liquid flow direction on a plane 0.038 m above the tray floor. The probe positions are shown in Figure 5. Average linear liquid velocities were calculated

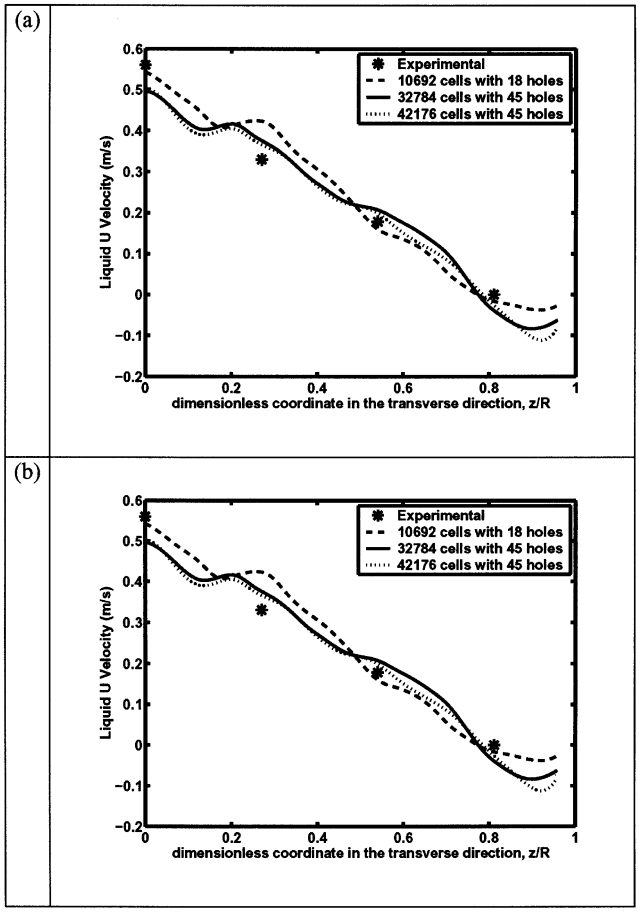

Figure 4. Sensitivity of the liquid-velocity profile prediction to grid spacing, and hole number and size (CFX4.4), $Q_L = 17.8 \times 10^{-3}$ m^3/s, $F_S = 0.462$: (a) upstream profile; (b) downstream profile.

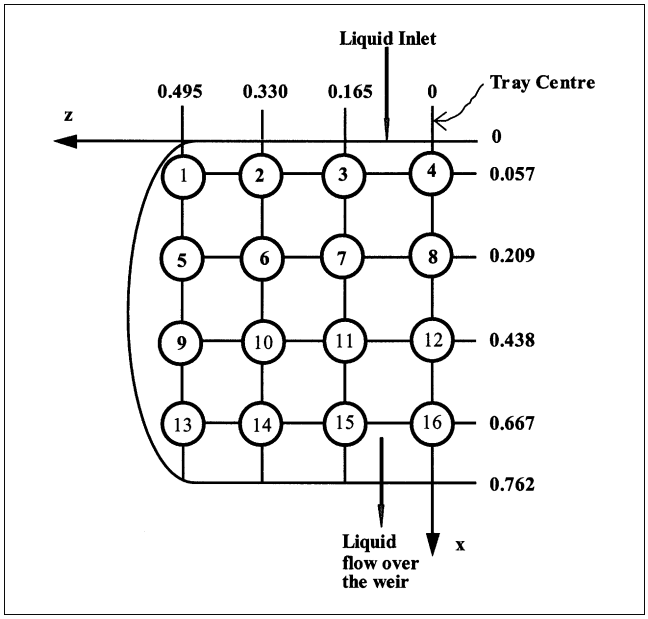

Figure 5. Experimental probe positions of Solari and Bell (1986).

All measurements are in meters. The plane of the probes is at an elevation of 0.038 m above the tray floor.

by dividing the distance between two rows of probes by the time elapsed for the dye to cover this distance. In our model geometry, probes 5 to 8 lie on $x = 0.209$ m and probes 9 to 12 lie on $x = 0.438$ m. In order to compare the experimental measurements with the CFD predictions, line integrals of the horizontal component of the liquid velocity were taken on the plane $y = 0.038$ m between $x = 0.209$ and $x = 0.438$ m. The resulting velocity profiles have been referred to as upstream profiles. Similarly, line intergrals were taken between $x = 0.438$ and $x = 0.667$ m for the measurements made between the middle of the tray and the outlet weir, with the resulting velocity profiles designated as downstream profiles. From Figure 4, it is clear that no significant improvements are observed in the simulation results as the numbers of cells and holes are increased.

Using CFX5.4, where the mesh was unstructured, it was possible to get results for the actual number of holes. As shown in Figure 6, the liquid-velocity profile curves are closer to the experimental values for the finer mesh with the actual number of holes, although the improvements are not very significant. Not unexpectedly, both CFX4.4 and CFX5.4 predict similar liquid-velocity profiles. The physical models are exactly the same in both versions of the simulator.

Velocity distributions

In Figures 6 to 9, liquid horizontal velocities predicted by the CFD simulations are compared against the experimental data of Solari and Bell (1986) for a range of operating conditions. Since the inlet velocity profiles were not characterized in their experiments, we consider a few alternate specifications for the inlet velocity profile. A parabolic liquid inlet velocity profile was used for most of the simulations, while a flat profile was used in a few cases to assess the sensitivity of

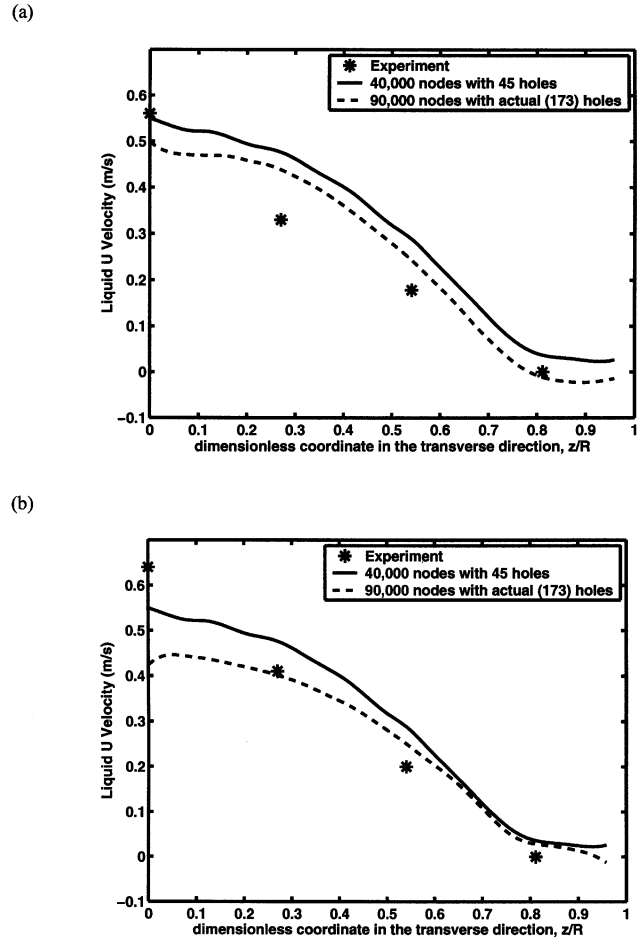

Figure 6. Liquid-velocity profile, $Q_L = 17.8 \times 10^{-3}$ m^3/s, $F_s = 0.462$ (CFX5.4): (a) upstream profile; (b) downstream profile.

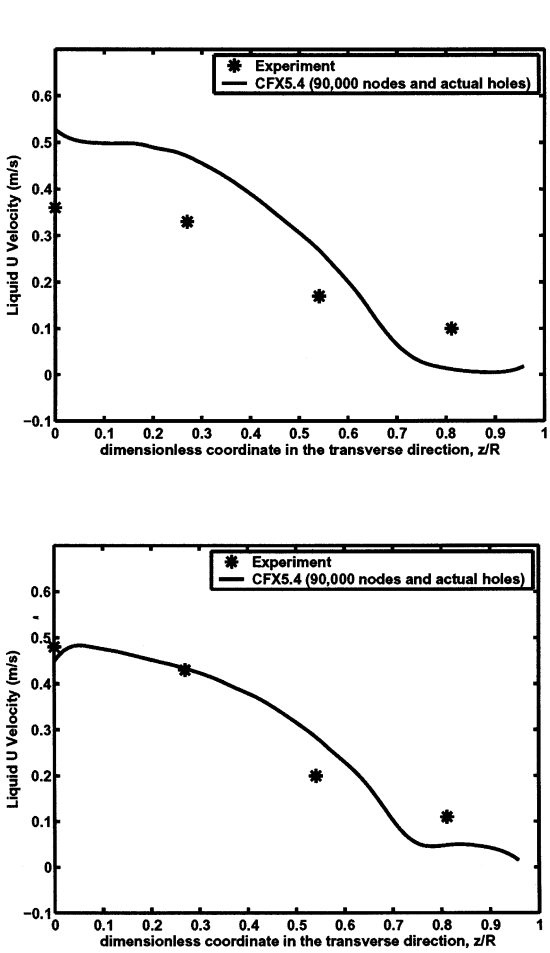

Figure 7. Liquid-velocity profile, $Q_L = 17.8 \times 10^{-3}$ m^3/s, $F_S = 0.801$ (CFX5.4): (a) upstream profile; (b) downstream profile.

the flow profiles to the inlet conditions. The predictions are generally in good agreement with the experimental data. It has been observed that (Kister, 1992) at very low liquid rates, the liquid inlet velocity profile has a strong influence on the liquid flow profile within the tray. In the single-phase modeling work, a flat inlet profile was recommended for low values of the flow parameter, F_{LV} ($F_{LV} < 0.25$). As Figure 8 shows, the parabolic and flat inlet profiles give comparable results at $F_S = 1.015$, for which the flow parameter ($F_{LV} = 0.25$) is on the borderline of the previous recommendation. A flat inlet profile was used for the gas and liquid loads where $F_{LV} < 0.25$. In general, it can be concluded that the liquid *inlet velocity profile* should be a function of the liquid flow rates and that it should have a significant effect on the evolution of the flow in the interior of the tray. The uncertainties in the specification of this inlet boundary condition (which are often not well characterized in experiments) might be one of the reasons for some of the discrepancies observed between the CFD predictions and the experimental data. The liquid-velocity profiles also will be affected by the liquid holdup fraction and drag coefficient correlations used in estimating the interphase drag term. Other sources of error, but less significant ones, are the grid resolution and the number and size of holes (as shown in Figures 4 and 6). Overall, the model predictions are not far from the experimental errors. The slight oscillations observed in the lower liquid rate velocity profiles are caused by a high gas rate rising through a small number of holes.

From the experimental studies that have been conducted so far, particularly from the works of Solari et al. (1982) and Solari and Bell (1986), a general understanding of the liquid flow pattern inside the trays has been developed, as summarized by Kister (1992). An assessment of the ability of the CFD model to predict the observations that have been made can be obtained with the help of the liquid-velocity profiles along specific lines, as presented earlier; a more complete picture emerges with the liquid-velocity vector plots shown in Figure 10. It should be noted that the liquid- (or gas-) velocity vector alone could be large even in zones where the corresponding liquid volume fraction is zero. Hence, the product of the liquid-velocity vector is plotted with the local liquid volume fraction, since it gives a true measure of local liquid flow rates. A nonuniform liquid-velocity distribution is observed in all cases. The liquid velocity decreases as one moves from the tray center toward the tray wall. Solari and Bell (1986) made similar observations. As Solari and Bell (1986) remarked, the gas rate plays an important role in determining the liquid-velocity distribution. The degrees of recircula-

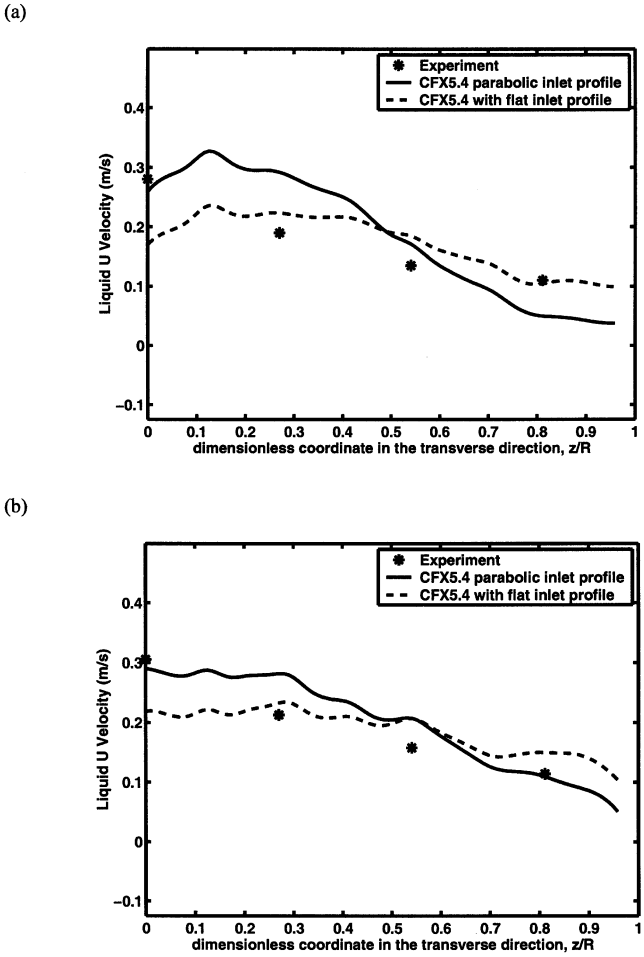

Figure 8. Liquid-velocity profile, $Q_L = 6.94 \times 10^{-3}$ m^3/s, $F_S = 1.015$ (CFX5.4): (a) upstream profile; (b) downstream profile.

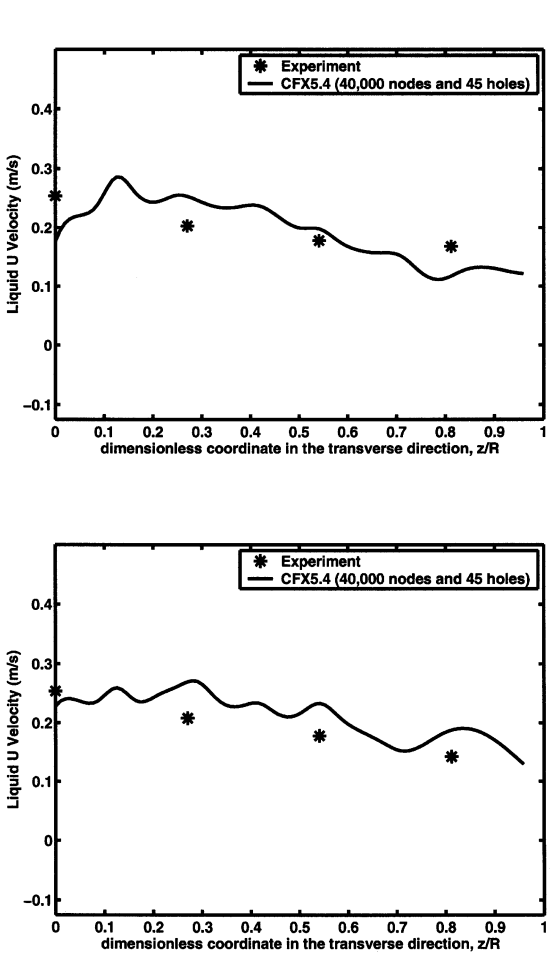

Figure 9. Liquid-velocity profile, $Q_L = 6.94 \times 10^{-3}$ m^3/s, $F_S = 1.464$ with a flat inlet profile (CFX5.4): (a) upstream profile; (b) downstream profile.

tion, channeling or stagnant zones that prevail depend on the gas rate. Having fewer holes (Figure 10b) results in a more uneven liquid distribution as compared to having more holes (Figure 10a). The liquid-velocity distribution in the transverse direction is more uniform at higher gas rates (compare Figures 10c and 10d), as the increased gas rate helps to distribute the liquid more evenly. The nonuniform liquid-velocity distribution in the transverse direction is more vivid at a higher liquid rate (Figure 10a). This is expected, since the given gas rate ($F_S = 0.462$) is high enough to shape the velocity distribution of the lower liquid rate, as Solari et al. (1982) observed. At low gas rate and high liquid rate (corresponding to Figure 10a), the two-phase model for the CFX4.4 simulation with 42,176 cells (not shown) tended to predict backward flow of liquid near the tray wall, although it was weak. Finer resolution of the grid spacing near the tray wall provided by the CFX5.4 mesh eliminated the backward flow, replacing it with a stagnant zone, as seen in Figure 10a. After performing additional dye injection tests, Solari and Bell concluded that this region was a stagnant region. The single-phase model at the given liquid and gas rate combination also predicted a stagnant zone. Comparing the vector plots for lower and higher liquid flow rates, the extent of liquid overshoot over the weir can be seen to be captured in a realistic manner in the simulations. For example, in Figure 10c, the velocity vector head is pointed downwards immediately past the weir, whereas in Figure 10a, the inertia at the higher liquid flow rates carries the fluid into the central zone of the downcomer.

Additional insight into gas and liquid flow behavior predicted by the CFD model can be gained with the aid of streamlines. Figure 11 shows liquid- and gas-phase streamlines for three different combinations of gas and liquid loads, giving a picture of how selected liquid- and gas-phase fluid particles flow from inlet to outlet. Turbulence and agitation by the gas phase (which is stronger at high gas rates; Figure 11b) force the liquid particles to follow wobbling paths. There is a noticeable circulation of liquid in the downcomer. The free-falling liquid impinging on the downcomer pool of liquid and floor, the narrow space in the downcomer, and the resistance to liquid flow caused by the narrow downcomer clearance are expected to cause this circulation. The downcomer circulation is in agreement with the commonly observed liquid flow behavior in single-pass cross-flow sieve trays as described by Lockett (1986). The effect of the liquid flow on the gas-phase streamlines is apparent from the bending of the

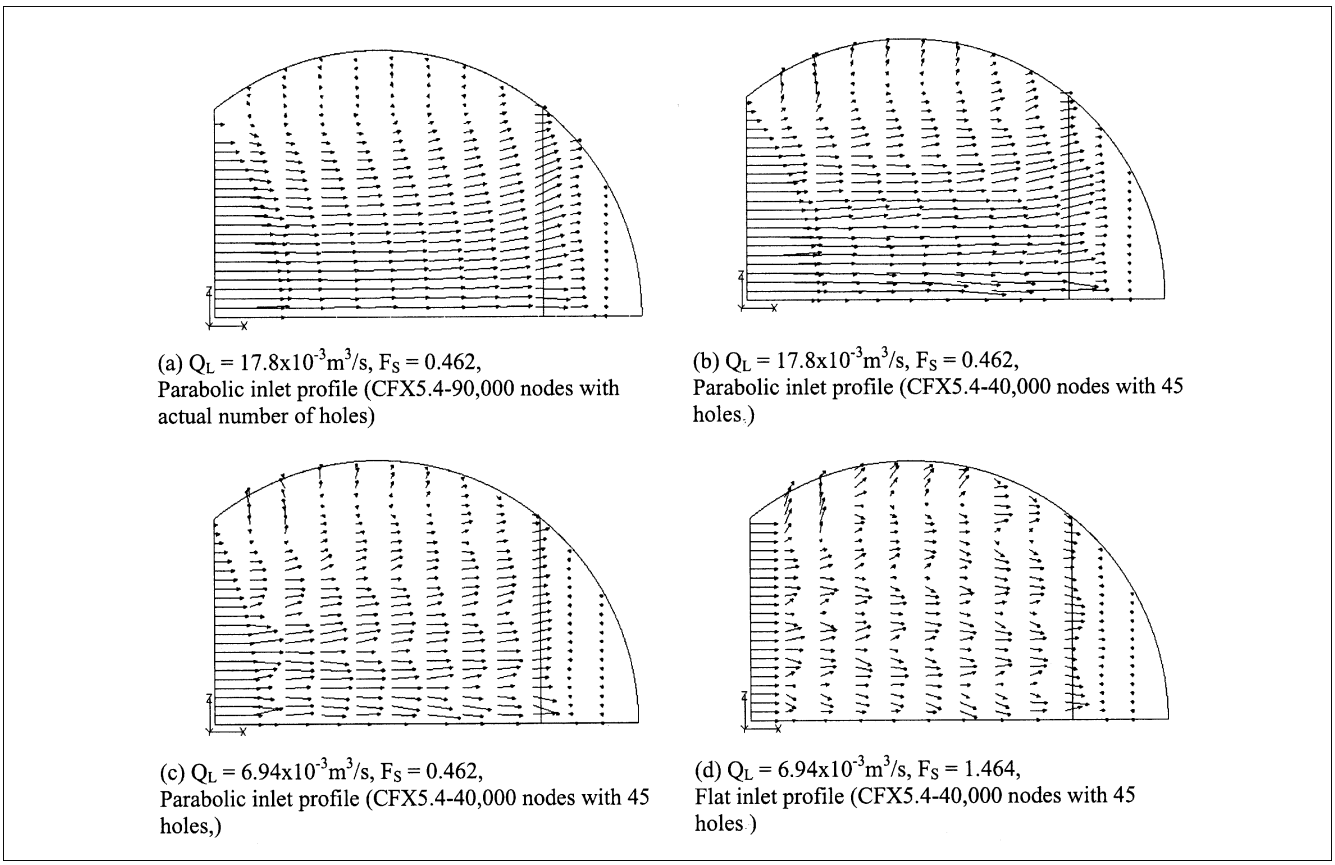

Figure 10. Liquid-velocity vector plots on the plane of the experimental probes. A modified liquid velocity vector, which is a product of the liquid velocity vector and the liquid volume fraction, was used in obtaining the magnitudes of the velocity vectors shown.

gas-phase streamlines in the direction of the liquid flow. The bending is more intense near the outlet weir because of the increased liquid velocities as liquid starts to fall down from the weir. At a low liquid rate (Figure 11c), the gas encounters almost no sideways push, and it appears to flow in a straight path. Likewise, small or no vertical displacements of the liquid streamlines are seen at lower gas rates (Figure 11a), whereas at higher gas rates (Figure 11b) the liquid is pushed up significantly. These figures also confirm the path of the liquid flow in the downcomer zone with varying liquid flow rates. At low liquid rates, the weir crest is smaller and the liquid flows nearer to the downcomer wall. With increasing gas and liquid rates, the liquid trajectory shows a clear overshoot in the downcomer zone.

A major advantage of the extension to the two-phase modeling is the availability of the gas-phase flow profiles. This is needed not only to get a measure of uniformity of the gas-phase flow profile, but also in simulating the interphase mass transfer, and, thus, calculating the Murphree tray efficiency, which is the next logical step in carrying out such detailed simulations. Selected profiles of the gas-phase vertical-component velocity are shown in Figure 12. In Figures 12a to 12c, the oscillations close to the tray floor correspond to the discrete distribution of holes. The magnitude of these oscillations decreases with increasing heights above the tray floor. As soon as the weir height is crossed, the gas velocity decreases owing to the increase in the cross-sectional area available for gas flow. The profile curves have maximum values directly above the inlet holes. There are four maxima corresponding to the four rows of holes encountered in sweeping from the tray center to the tray wall at $x = 0.32$ m. The triangular pitch arrangement of the holes results in differences in the number of holes encountered between the tray center and the tray wall at different values of x.

The longitudinal and transverse variations of the gas V velocity profiles are not significant, except for the slightly large values of the velocity at the tray center (Figure 12d). Thus, the model did not predict any significant gas-phase maldistribution. Figure 13 shows that the variation of the liquid-velocity profile, $U(z)$, in the vertical direction is small in the active regions of the froth, that is, from $y = 0.019$ m to $y = 0.15$ m. The two-phase modeling makes it possible to verify a hypothesis made in the single-phase modeling work of Mehta et al. (1998), viz., that the gas and liquid phases move with the same velocities in the longitudinal and transverse directions to liquid flow. As shown in Figure 14, the hypothesis is a reasonable one, since on average the gas and liquid U-component velocities have small differences in the active froth region of the sieve tray (such as $y = 0.15$ m). The differences are more pronounced, of course, close to the tray floor ($y = 0.038$ m).

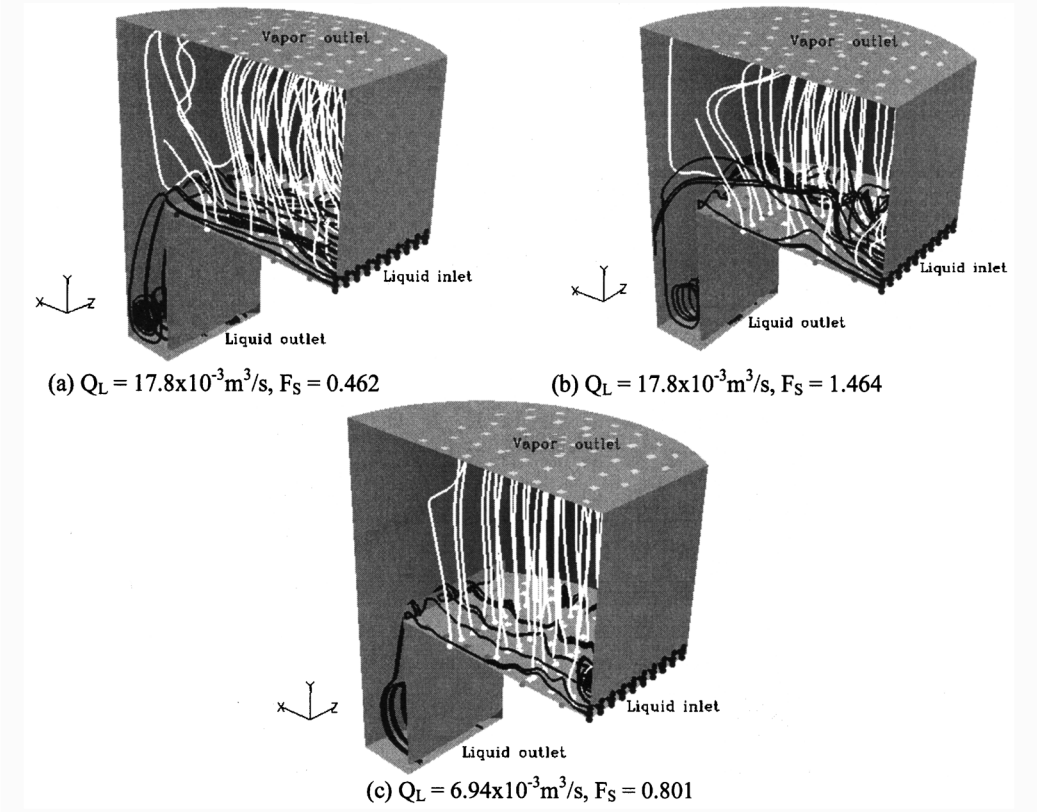

Figure 11. Selected streamline profiles of the liquid (in black) and the gas (in white).

Clear liquid height, froth height, and liquid holdup fraction in froth

Having validated the simulation results against the experimentally measured *liquid-velocity distributions*, we compute several macroscopic results, such as *clear-liquid height* and *froth height*, and compare them with existing correlations. It is essential that the CFD simulations predict the same trends as existing correlations, which have stood the test of time.

Clear-liquid height is defined as the height of liquid that would exist on the tray in the absence of vapor flow. Using this definition, the clear-liquid height has been calculated as the tray spacing multiplied by the volume average of the liquid volume fraction above the bubbling area of the tray floor. In Figures 15 and 16, predicted values of clear-liquid height are compared with values calculated using various correlations, including that proposed by Solari and Bell (1986). Note that the clear-liquid height is predicted to decrease with increasing F-factor at a given liquid flow rate (Figure 15), and it is expected to increase with the liquid flow rate at a given F-factor (Figure 16).

For trays operating in the froth regime, the correlations of Colwell (1979) and Bennett et al. (1983) are both good for clear-liquid height predictions. The CFD predictions are slightly larger than the values obtained using the Solari and Bell (1986) proposed correlation. Van Baten and Krishna (2000) also found the CFD to give clear-liquid height values that are larger than the experimental ones. They reasoned that this happened because the Bennett et al. correlation used in the interphase momentum drag term ignores coalescence caused by impurities.

It is known that the Bennett et al. (1983) correlation overpredicts the liquid holdup fraction in froth. From Eq. 13, at a given gas flow rate the use of the Bennett et al. (1983) correlation amounts to using a constant multiplier as a drag coefficient. This constant factor is inversely proportional to the average liquid holdup fraction, but it is proportional to the second power of the average gas holdup fraction. Overpredicting the average liquid holdup fraction results in a *reduction* in the interphase drag term. The gas then does not exert enough drag force on the liquid. This can be thought of as if the tray were operating at a slightly lower gas rate than the actual one, which results in a larger clear-liquid height. To verify this, we changed the gas holdup fraction correlation to that of Colwell's, which is known to work well in the froth region. In Figure 16 it is verified that the Bennett et al. correlation does indeed lead to larger clear-liquid height values as compared to Colwell's correlation. Other factors that can lead to the overprediction include insufficient spatial resolution of the flow near the tray floor, use of a small number of holes, and the use of large calming zones. Reducing the grid spacing in the vertical direction was not found to result in a significant change in the clear-liquid height value (see Figure 3). Use of a small number of holes is expected to lead to gas channeling, which can result in an increased clear-liquid

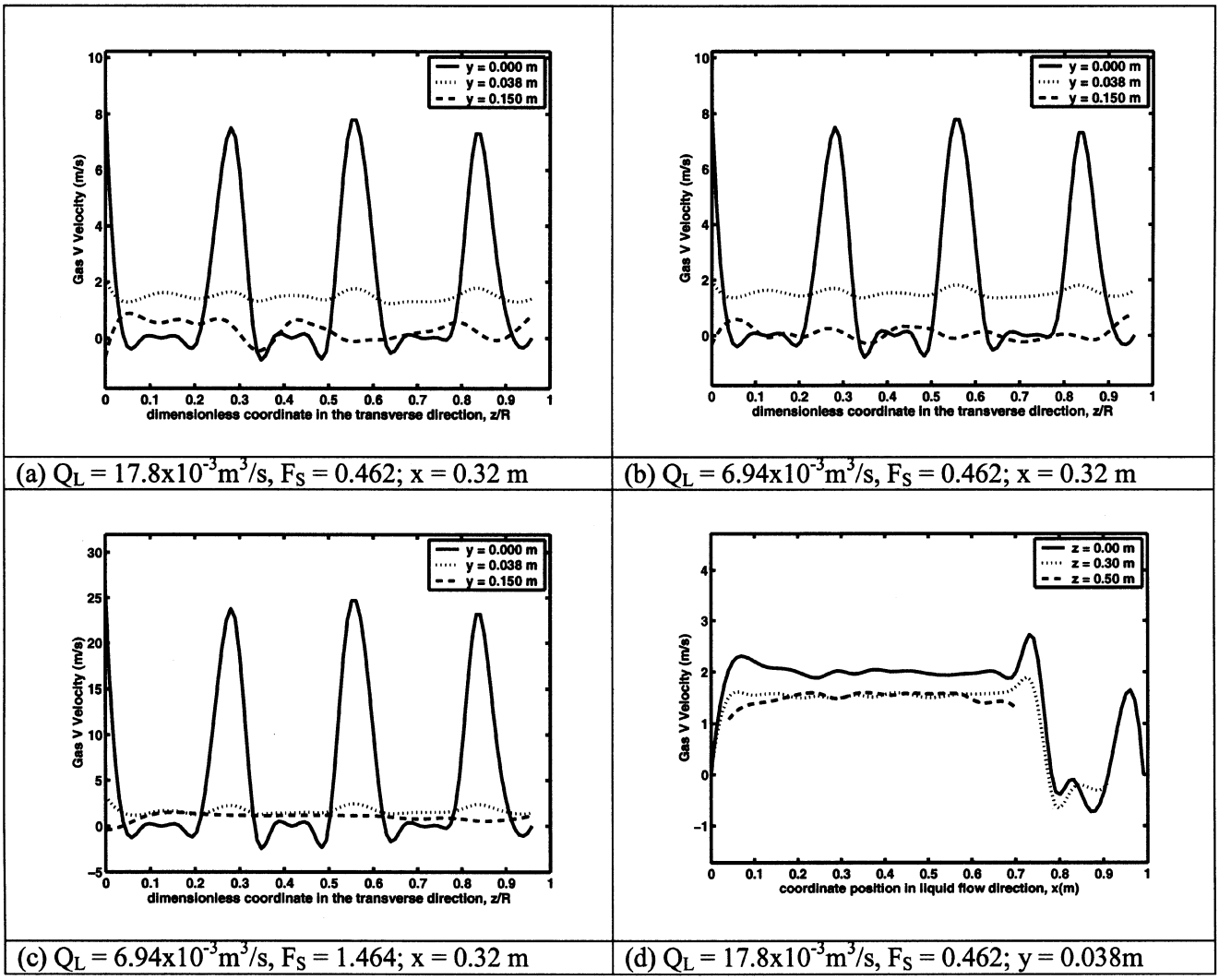

Figure 12. (a) to (c) Gas *V* velocity profiles at different elevations above tray floor; (d) gas *V* velocity profiles in the longitudinal direction to the liquid flow.

height. Large calming zones have a similar effect as that of using a small number of holes.

The froth region is usually defined as the region in which the liquid volume fraction is greater than 10%. The average froth height has been calculated as the area average (over the tray deck–(x,z) plane) of the vertical distance (y) from the tray floor at which the liquid volume fraction starts to fall below 10%. Liquid holdup fraction in froth is often defined as the ratio of clear-liquid height to froth height. In conventional sieve tray design and analysis, not all of the three parameters—clear-liquid height, froth height, and average liquid holdup fraction—are independent. Given any two of the three, say, clear-liquid height and liquid holdup fraction in froth, the third can be calculated (froth height is the ratio of clear-liquid height to liquid holdup fraction in froth). The CFD simulation allows all the three parameters to be determined independently, provided one uses a cutoff value of 10% in defining the froth regime. For the liquid holdup fraction, two approaches were followed. One was as the ratio of clear-liquid height to froth height, and the other as the volume average of the liquid volume fraction in froth. In either case, we had to make use of the 10% value as the lower limit for the liquid volume fraction in the froth region. Both approaches gave results that are very close to each other, as shown in Figure 17. This validates the 10% cutoff value used in defining the froth region.

Predicted values of the average liquid holdup fraction in froth compared with correlations recommended for this parameter are shown in Figure 17. The CFD simulation gives values that are very close to the values calculated using the Bennett et al. (1983) correlation. Froth-height prediction results are shown in Figure 18. Comparisons are made with two correlations. Here again the use of the Bennett et al. correlation is expected to lead to a shorter froth height, since the gas is not exerting enough force to expand the liquid as high as it should. Taking into account the many uncertainties involved in the correlations used to estimate these parameters, the CFD predictions are quite acceptable.

More profiles of volume-fraction-dependent quantities are given in Figures 19 to 21. Figure 19 shows shaded contour

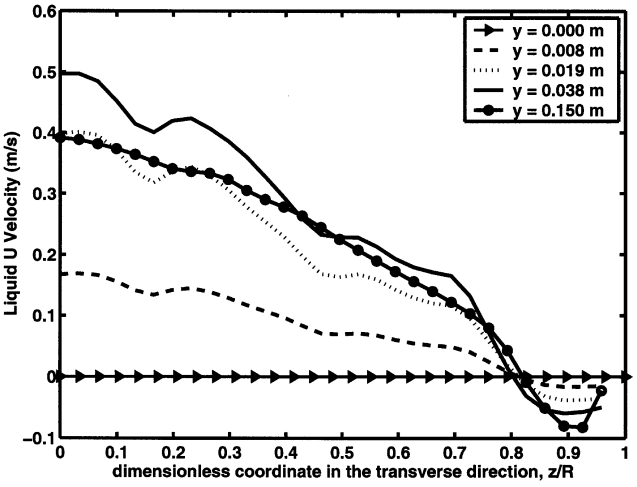

Figure 13. Average liquid *U* velocity profiles at different elevations above tray floor.

Average taken between $x = 0.209$ m and $x = 0.438$ m, $Q_L = 17.8 \times 10^{-3}$ m^3/s, $F_s = 0.801$ (from CFX4.4 32,784 cells and 45 holes).

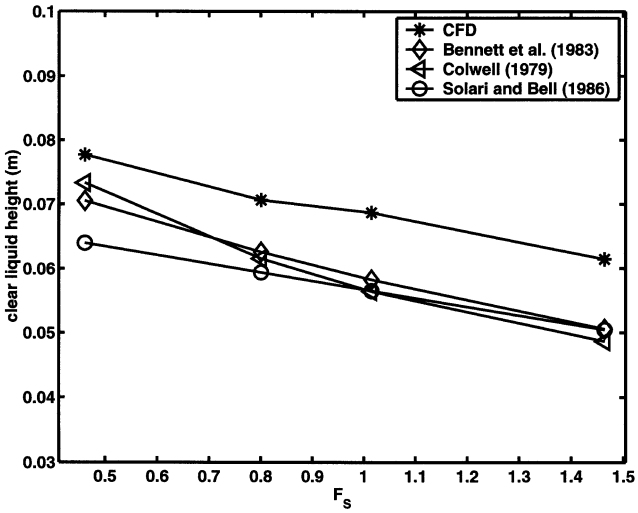

Figure 15. Clear-liquid height as a function of *F*-factor, F_S, $Q_L = 17.8 \times 10^{-3}$ m^3/s.

plots of liquid volume fraction profiles on a vertical plane 0.01 m from the tray center. Almost all the liquid resides near the tray floor. No weeping is expected, since the way the CFD imposes and solves boundary conditions does not allow this. From the weir height up, the liquid presence diminishes rapidly until it suddenly seems to disappear, leaving most of the tray space to be filled with the gas phase. The gas is seen reducing the liquid volume fraction around the gas inlet holes as it finds a way up through the pool of liquid on the tray floor. The dispersion density of the froth is more uniform for the actual number of holes (Figure 19c). At a high gas rate (Figure 19d), the expansion of the froth height and the reduction of the average liquid holdup fraction above the tray floor are more pronounced than those at lower gas rates (Figure 19b).

Figure 20 shows dispersion height vs. liquid dispersion density profiles. For a given liquid rate, the dispersion density decreases while the dispersion height increases as the gas rate is increased. Clear-liquid height profiles determined from averages of the liquid volume fraction on vertical slices above the tray floor are shown in Figure 21. The clear-liquid heights are larger near the liquid entrance and the outlet weir, supporting the explanation made earlier concerning the effect of calming zones. Similarly, larger clear-liquid heights are seen at the tray center and near the tray wall where there are no gas inlet holes.

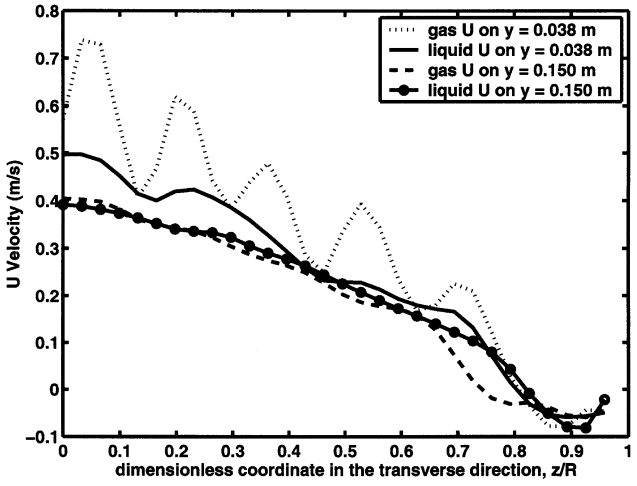

Figure 14. Average gas and liquid *U* velocity profiles at different elevations above tray floor.

Averages taken between $x = 0.209$ m and $x = 0.438$ m, $Q_L = 17.8 \times 10^{-3}$ m^3/s, $F_S = 0.801$ (from CFX4.4 32,784 cells and 45 holes).

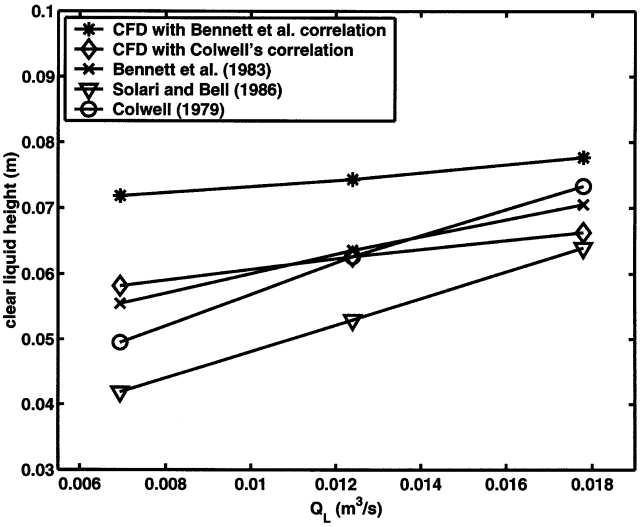

Figure 16. Clear-liquid height as a function of liquid rate, Q_L, $F_S = 0.462$.

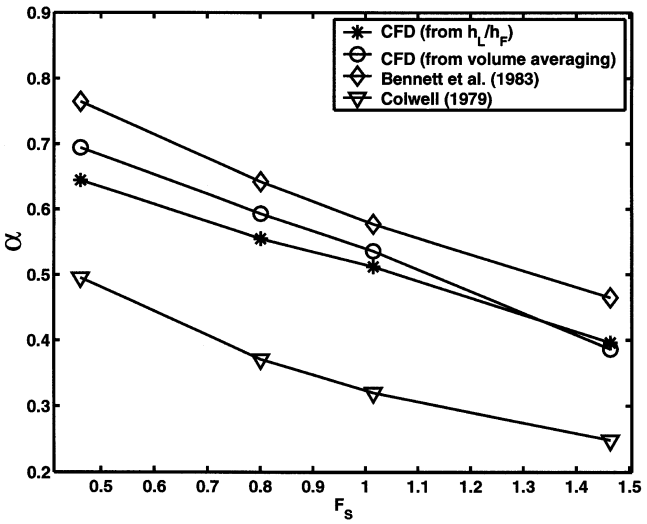

Figure 17. Average liquid holdup fraction in froth as a function of *F*-factor, F_S, $Q_L = 17.8 \times 10^{-3}$ m^3/s.

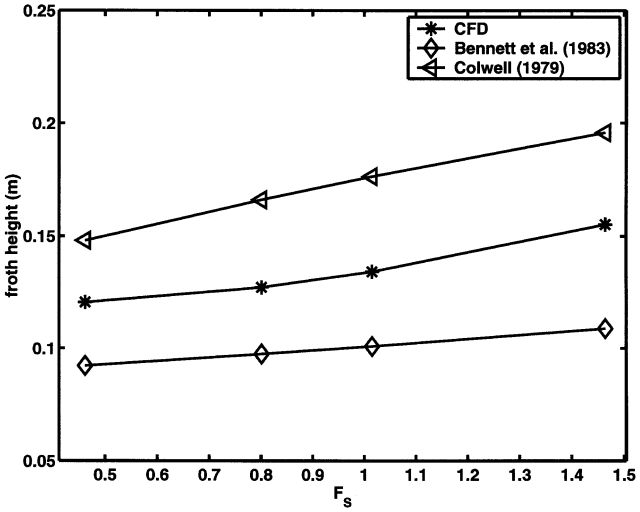

Figure 18. Average froth height, h_F, as a function of *F*-factor, F_S, $Q_L = 17.8 \times 10^{-3}$ m^3/s.

Conclusion

In this work we have attempted to predict the flow pattersn and hydraulics of a commercial-scale sieve tray by means of computational fluid dynamics (CFD). The flow inside the tray was modeled as a three-dimensional two-phase flow of gas and liquid in the Eulerian–Eulerian framework. The time- and volume-averaged continuity and momentum equations were numerically solved using the commercial packages CFX5.4 and CFX4.4 of AEA Technology. The gas- and liquid-phase equations were coupled through an interphase mo-

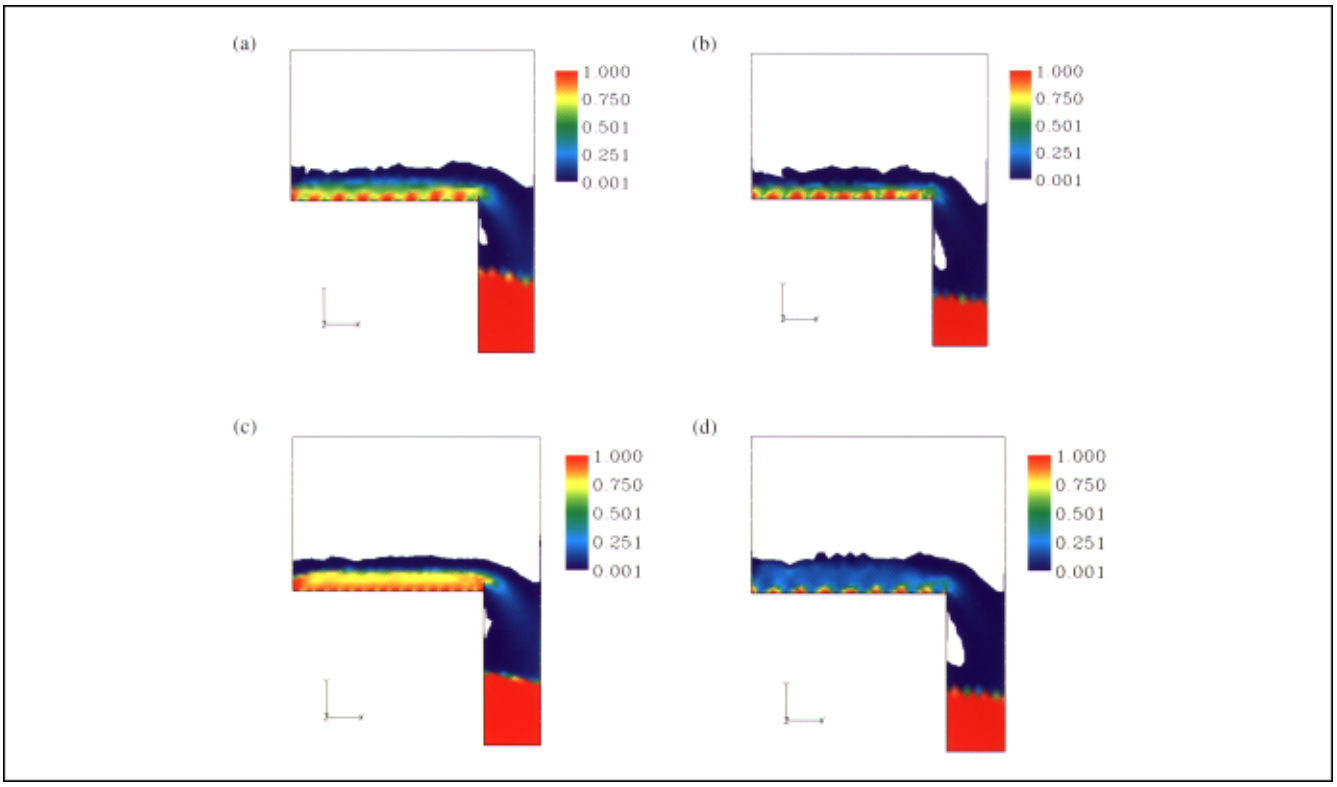

Figure 19. Liquid volume fraction profiles on a vertical section 0.01 m from the tray center.

(a) $Q_L = 17.8 \times 10^{-3}$ m^3/s, $F_S = 0.462$ (40,000 nodes with 45 holes); (b) $Q_L = 6.94 \times 10^{-3}$ m^3/s, $F_S = 0.462$ (40,000 nodes with 45 holes); (c) $Q_L = 17.8 \times 10^{-3}$ m^3/s, $F_S = 0.462$ (90,000 nodes with actual number of holes); (d) $Q_L = 6.94 \times 10^{-3}$ m^3/s, $F_S = 1.464$ (40,000 nodes with 45 holes).

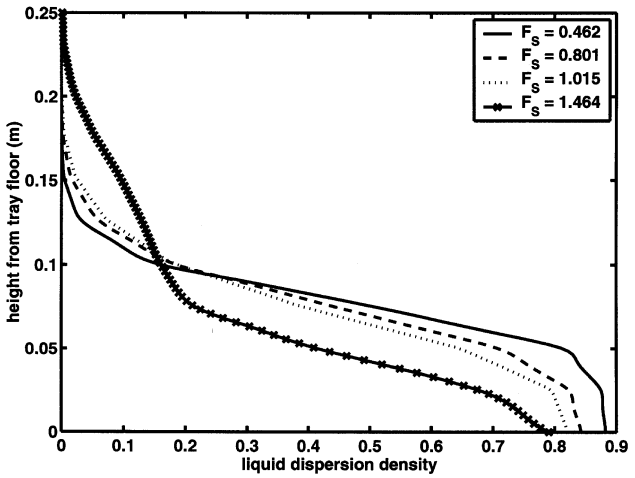

Figure 20. Dispersion height vs. liquid dispersion density profile, $Q_L = 6.94 \times 10^{-3}$ m^3/s.

mentum transfer term that was estimated locally using the drag coefficient correlation of Krishna et al. (1999) and the Bennett et al. (1983) liquid holdup fraction correlation. The CFD was used to predict velocity distributions, clear-liquid height, froth height, and liquid holdup fraction in froth for various combinations of gas and liquid rates. The simulation results exhibit all of the known features of the two-phase flow field in sieve trays and are in good agreement with the experimental results of Solari and Bell (1986). In the next phase of the study we can explore residence-time distributions in both the gas and liquid phases, as well as study the interphase mass transfer with the aim of predicting the Murphree tray efficiency.

Experiments for trays have proved to be expensive and time-consuming. That is why only very few attempts have been made so far to determine fluid flow patterns inside trays. Modeling using CFD overcomes many of the limitations associated with the experiments. Of paramount importance are its capability to give complete information and the ease with which one can change tray geometry and operating conditions without incurring appreciable cost. From this work, we conclude that even with a simple interphase transfer model, we were able to get results that closely match the experimental data. With more refined models, such as a more accurate interphase momentum transfer relation and the inclusion of interphase mass transfer, we expect to get more accurate predictions. The results of this work show that CFD can be used as an invaluable tool in the design and analysis of industrial trays.

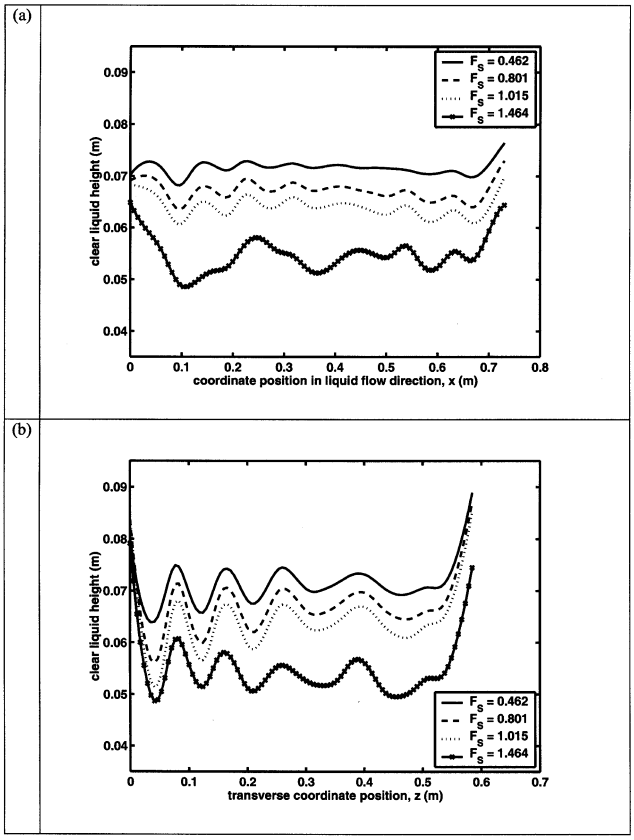

Figure 21. Clear-liquid height profiles in longitudinal and transverse directions to liquid flow, $Q_L = 6.94 \times 10^{-3}$ m^3/s: (a) averaged in the *y*- and *z*-directions; (b) averaged in the *x*- and *y*-directions.

Acknowledgment

Financial support from NSERC is gratefully acknowledged. Our work made use of the infrastructure and resources of MACI (Multimedia Advanced Computational Infrastructure), funded in part by the CFI (Canada Foundation for Innovation), ISRIP (Alberta Innovation and Science Research Investment Program), and the Universities of Alberta and Calgary.

Notation

A_B = tray bubbling area, m^2
A_H = total area of holes, m^2
C_D = drag coefficient
d_G = bubble diameter, m
F_{LV} = flow parameter = $L/G\sqrt{\rho_G/\rho_L}$, L, G = liquid, gas mass flow rate, respectively
F_S = F factor = $V_S\sqrt{\rho_G}$
h_F = froth height, m
h_L = clear liquid height, m
$\boldsymbol{M}_{GL}$ = interphase momentum transfer, kg·m^{-2}·s^{-2}
p_G = gas-phase pressure, N·m^{-2}
p_L = liquid-phase pressure, N·m^{-2}
Q_L = liquid volumetric flow rate, m^3/s
r_G = gas-phase volume fraction
r_G^{average} = average gas holdup fraction in froth
r_L = liquid-phase volume fraction
U = x-component of velocity, m/s
V = y-component of velocity, m/s
W = z-component of velocity, m/s
$\boldsymbol{V}_G$ = gas-phase velocity vector, m/s
$\boldsymbol{V}_L$ = liquid-phase velocity vector, m/s
V_S = gas-phase superficial velocity based on bubbling area, m/s
V_{slip} = slip velocity, m/s
x = coordinate position in the direction of liquid flow across tray, m
y = coordinate position in the direction of vapor flow, m
z = coordinate position in the transverse direction to liquid flow, m

Greek letters

α = average liquid holdup fraction in froth
$\mu_{\text{eff},G}$ = effective viscosity of gas, kg·m^{-1}·s^{-1}

$\mu_{\text{eff},L}$ = effective viscosity of liquid, $\text{kg}\cdot\text{m}^{-1}\cdot\text{s}^{-1}$
ρ_G = gas-phase density, kg/m^3
ρ_L = liquid-phase density, kg/m^3

Literature Cited

Banerjee, S., "Modelling Considerations for Turbulent Multiphase Flows," *Engineering Turbulence Modelling and Experiments: Proceedings of the International Symposium on Engineering Turbulence Modelling and Measurements*, W. Rodi and E. N. Ganic, eds., Dobrovnik, Yugoslavia (1990).

Bell, R. L., "Experimental Determination of Residence Time Distributions on Commercial Scale Trays Using a Fibre Optic Technique," *AIChE J.*, **18**, 491 (1972).

Bell, R. L., and R. B. Solari, "Effect of Nonuniform Velocity Fields and Retrograde Flow on Distillation Tray Efficiency," *AIChE J.*, **20**, 688 (1974).

Bennett, D. L., Rakesh Agrawal, and P. J. Cook, "New Pressure Drop Correlation for Sieve Tray Distillation Columns," *AIChE J.*, **29**, 434 (1983).

Borchers, O., C. Busch, A. Sokolichin, and G. Eigenberger, "Applicability of the Standard k-ϵ Turbulence Model to the Dynamic Simulation of Bubble Columns: II. Comparison of Detailed Experiments and Flow Simulations," *Chem. Eng. Sci.*, **54**, 5927 (1999).

Colwell, C. J., "Clear Liquid Height and Froth Density on Sieve Trays," *Ind. Eng. Chem. Proc. Des. Dev.*, **20**, 298 (1979).

Crowe, C., M. Sommerfield, and Y. Tsuji, *Multiphase Flows with Droplets and Particles*, CRC Press, Boca Raton, FL (1998).

Fischer, C. H., and J. L. Quarini, "Three-Dimensional Heterogeneous Modelling of Distillation Tray Hydraulics," AIChE Meeting, Miami Beach, FL (1998).

Gidaspow, D., *Multiphase Flow and Fluidization*, Academic Press, New York (1994).

Jacobsen, H. A., B. H. Sanæs, S. Grevskott, and H. F. Svendson, "Modelling of Vertically Bubble-Driven Flows," *Ind. Eng. Chem. Res.*, **36**, 4052 (1997).

Kister, H. Z., *Distillation Design*, McGraw-Hill, New York (1992).

Krishna, R., M. I. Urseanu, J. M. van Baten, and J. Ellenberger, "Rise Velocity of a Swarm of Large Gas Bubbles in Liquids," *Chem. Eng. Sci.*, **54**, 171 (1999a).

Krishna, R., J. M. van Baten, J. Ellenberger, A. P. Higler, and R. Taylor, "CFD Simulations of Sieve Tray Hydrodynamics," *Chem. Eng. Res. Des., Trans. Inst. Chem. Eng.*, **77**, 639 (1999b).

Libby, P. A., *Introduction to Turbulence*, Taylor & Francis, Washington, DC (1998).

Liu, C. J., X. G. Yuan, K. T. Yu, and X. J. Zhu, "A Fluid-Dynamic Model for Flow Pattern on a Distillation Tray," *Chem. Eng. Sci.*, **55**, 2287 (1999).

Lockett, M. J., *Distillation Tray Fundamentals*, Cambridge Univ. Press, Cambridge (1986).

Mehta, B., K. T. Chuang, K. Nandakumar, "Model for Liquid Phase Flow on Sieve Trays," *Chem. Eng. Res. Des., Trans. Inst. Chem. Eng.*, **76**, 843 (1998).

Pope, S. B., *Turbulent Flows*, Cambridge Univ. Press, Cambridge (2000).

Porter, K. E., M. J. Lockett, and C. T. Lim, "The Effect of Liquid Channelling on Distillation Plate Efficiency," *Trans. Inst. Chem. Eng.*, **50**, 91 (1972).

Salas, M. D., J. N. Hefner, and L. Sakell, *Modelling Complex Turbulent Flows*, Kluwer, Boston (1999).

Sohlo, J. J., and S. Kinnunen, "Dispersion and Flow Phenomena on a Sieve Plate," *Trans. Inst. Chem. Eng.*, **55**, 71 (1977).

Solari, R. B., and R. L. Bell, "Fluid Flow Patterns and Velocity Distribution on Commercial-Scale Sieve Trays," *AIChE J.*, **32**, 640 (1986).

Solari, R. B., and R. L. Bell, "The Effect of Transverse Eddy Dispersion on Distillation Efficiency," AIChE Meeting, Atlanta, GA (1978).

Solari, R. B., E. Saez, I. D'apollo, and A. Bellet, "Velocity Distribution and Liquid Flow Patterns on Industrial Sieve Trays," *Chem. Eng. Commun.*, **13**, 369 (1982).

Van Baten, J. M., and R. Krishna, "Modelling Sieve Tray Hydraulics Using Computational Fluid Dynamics," *Chem. Eng. J.*, **77**, 143 (2000).

Van Leer, B., "Towards the Ultimate Conservation Difference Scheme, II: Monotonicity and Conservation Combined in a Second-Order Scheme," *J. Comput. Phys.*, **14**, 361 (1974).

Weiler, D. W., W. V. Delniki, and B. L. England, "Flow Hydraulics of Large-Diameter Trays," *Chem. Eng. Prog.*, **69**, 67 (1973).

Wilcox, D. C., *Turbulence Modelling for CFD*, DCW Industries Inc., La Cañada, CA (1993).

Manuscript received Feb. 22, 2002, and revision received Sept. 30, 2002.